Substitution of Tyrosine Residues at the Aromatic Cluster around the βA−βB Loop of Rubisco Small Subunit Affects the Structural Stability of the Enzyme and the in Vivo Degradation under Stress Conditions†

Maria Gloria Esquível,*,‡ Teresa S. Pinto,‡ Julia Marín-Navarro,§ and Joaquín Moreno§

Department of Botany and Biological Engineering, Technical University of Lisbon, Lisbon P-1349-017, Portugal, and Department of Biochemistry and Molecular Biology, University of Valencia, Burjassot E-46100, Spain

Received December 20, 2005; Revised Manuscript Received February 25, 2006

ABSTRACT: Ribulose 1,5-bisphosphate carboxylase/oxygenase (rubisco) plays a central metabolic role in photosynthetic eukaryotes, and its catabolism is a crucial process for the nutrient economy of higher plants. The rubisco holoenzyme is assembled from eight chloroplast-encoded large subunits and eight nuclear-encoded small subunits. We have identified a cluster of conserved tyrosines at the interface between subunits (comprising Y67, Y68, and Y72 from the βA−βB loop of the small subunit and Y226 from the large subunit) that may contribute to holoenzyme stability. To investigate the role of these tyrosines in rubisco structure and in vivo degradation, we have examined site-directed mutants of these residues (Y67A, Y68A, Y72A, and Y226L) in *Chlamydomonas reinhardtii*. Even if all mutant strains were able to grow photoautotrophycally, they exhibited a reduction in rubisco activity and/or the level of expression, especially the Y67A and Y72A mutants. Besides, all mutant rubiscos were inactivated at a lower temperature than the wild type. The kinetics of proteolysis of the mutant enzymes with subtilisin revealed structural alterations, leading to facilitated disassembly (in the cases of Y67A and Y72A) or aggregation propensity (for Y68A and Y226L). When subjected to oxidative stress in vivo through exposure of liquid cultures to hydrogen peroxide, all mutant strains degraded rubisco at a faster rate than the wild type. These results demonstrate that the tyrosine cluster around the βA−βB loop of rubisco small subunit plays a stabilizing role by affecting the catalytic activity and the degradation rate of the enzyme in stressed cells.

Ribulose 1,5-bisphosphate carboxylase/oxygenase (EC 4.1.1.39, rubisco)[1] catalyzes the initial step of carbon metabolism, the fixation of carbon dioxide, in photosynthetic eukaryotes. The enzyme found in the chloroplast of green algae and higher plants has eight large subunits, containing the active site, and eight small subunits (reviewed in ref *1*). Large subunits are arranged as a tetramer of dimers around a central solvent channel, thereby defining a 4-fold symmetry axis. Small subunits are disposed as two tetramers at polar positions around that axis. Small subunits exhibit more sequence divergence between species than large subunits. In particular, the loop between β-strands A and B (A−B loop) of the small subunit shows high variability. This loop projects into the central solvent channel of the holoenzyme, making contacts with both large subunits and other small subunits (*2*), and has gained attention as an "assembly domain" (*3*−*5*). The A−B loop has only 10 residues in prokaryotes and nongreen algae, but higher plants have 22 residues and green algae 28 (*5*). In *Chlamydomonas reinhardtii*, a unicellular green algae, the A−B loop has six additional residues compared to land plants which cause a narrowing of the entrance to the solvent channel that passes through the center of the rubisco holoenzyme (*6*, *7*). Recently, it has been shown that the A−B loop of the small subunit can influence catalytic efficiency, CO_2/O_2 specificity, and holoenzyme stability (*8*), thereby renewing the interest in studying this region. The A−B loop of the *C. reinhardtii* rubisco contains several aromatic residues in proximity, integrating an aromatic cluster together with other residues from the large subunit. This cluster may contribute to the structural stability and subunit cohesion within the holoenzyme.

On the other hand, the eukaryotic rubisco is an extraordinarily abundant protein, its synthesis consuming a substantial portion of the nutrient resources (especially of nitrogen, of which rubisco allocates approximately one-fourth of the total content of a typical mature leaf) (*9*). In its turn, rubisco catabolism has a considerable impact on carbon, nitrogen, and sulfur economy in plants (*10*), as the precise timing of rubisco degradation influences the redistribution

† This work has been supported in part by an Integrative Action (E-37/02-HP2001-0018) between the University of Valencia, Spain, and the Technical University of Lisbon, Portugal, and Grants POCTI/AGG/46960/2002 from the Portuguese FCT-MCES and BMC2003-03209 from the Spanish DGESIC-MCYT.

* To whom correspondence should be addressed. E-mail: gesquivel@isa.utl.pt. Telephone: 213653176. Fax: 213653228.

‡ Technical University of Lisbon.

§ University of Valencia.

[1] Abbreviations: A−B loop, βA/βB loop; FPLC, fast protein liquid chromatography; LS, rubisco large subunit; PAGE, polyacrylamide gel electrophoresis; PAGGE, polyacrylamide gradient gel electrophoresis; PMSF, phenylmethanesulfonyl fluoride; PVDF, polyvinyldifluoridene; rubisco, D-ribulose-1,5-bisphosphate carboxylase/oxygenase; SDS, sodium dodecyl sulfate.

10.1021/bi052588y CCC: $33.50
Published on Web 04/13/2006

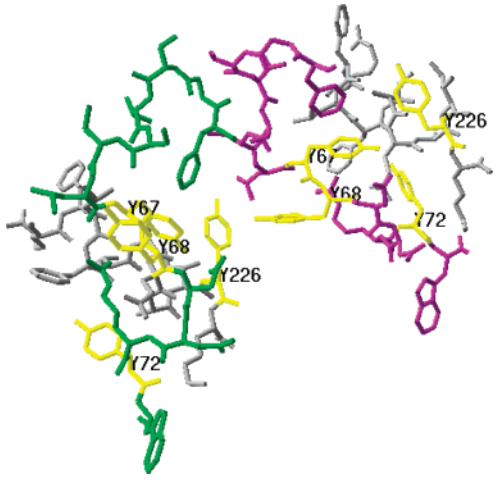

FIGURE 1: Aromatic cluster around the A−B loop. The residues between F60 and W73 from the A−B loop are shown for two small subunits (colored green and violet). Residues F218−K227 (part of α-helix 2) from two neighboring large subunits are colored gray. The studied tyrosine residues are colored yellow. The image is derived from the data of the X-ray crystal structure of *C. reinhardtii* rubisco (PDB entry 1GK8).

of nutrients within the organism during natural or stress-induced senescence. Several studies have shown that rubisco is oxidized prior to being degraded (*11*−*14*). One of the targets of oxidative modification is the cysteine thiol groups, and it has been suggested that thiol redox state may regulate rubisco turnover in vivo (*15*). Indeed, the replacement of a conserved cysteine (C172) of the large subunit has been shown to delay the stress-induced degradation of rubisco in vivo (*16*, *17*). More recently, the mutation of the vicinal C449 and C459 residues has been shown to enhance the binding of the oxidized rubisco to membranes (*18*), one of the steps preceding degradation in rubisco catabolism (*10*). Altogether, these results have demonstrated the feasibility of manipulating the in vivo degradation of rubisco through site-directed mutation of the redox-sensitive cysteine residues. Nevertheless, it is conceivable that the rubisco catabolism might also be altered by exchanging residues that affect the structural stability of the holoenzyme. In this work, we have investigated this possibility. We have focused our attention on the tyrosine cluster at the end of the A−B loop of the small subunit of rubisco, essentially formed by three conserved tyrosine residues from the small subunit (Y67, Y68, and Y72) and Y226 from the large subunit that interacts closely with amino acid residues from the A−B loop (Figure 1). We have examined site-directed mutants of these tyrosines in *C. reinhardtii* looking for structural alterations (as detected by changes in thermal stability and the kinetics of proteolytic fragmentation of the enzyme in vitro) and their consequences with respect to the degradation rate of the mutant rubiscos under stress conditions.

MATERIALS AND METHODS

Strains and Culture Conditions. C. reinhardtii rubisco mutant 18-7G *mt*+, which carries an *rbc*L nonsense mutation, does not synthesize the rubisco holoenzyme, and requires acetate for growth (*19*), was used as a host for transformation of the Y226L mutation. The *RbcS*Δ-T60-3 *mt*− strain, which lacks the small subunit gene family and also requires acetate for growth (*20*), was the host for Y67A, Y68A, and Y72A. In all cases, the host strains were transformed in parallel with a wild-type *rbc*L or *Rbc*S gene, producing wild-type transformants (termed L-Wt, S1-Wt, and S2-Wt) that were used as controls.

All strains were maintained at 25 °C in the dark with medium containing 10 mM acetate and 1.5% Bacto-agar (*21*). For biochemical analysis, cells were grown in liquid acetate medium on a rotary shaker under continuous white light (10 μE m^{-2} s^{-1}) at 25 °C. Cells were counted with a hemacytometer and were harvested at the beginning of the stationary phase (~10^7 cells/mL).

Directed Mutagenesis and Transformation. The Y226L mutagenesis of the chloroplast-encoded large subunit of rubisco was carried out as previously described (*16*). A 2669 bp *Hpa*I DNA fragment containing the entire *rbcL* gene (*22*) was cloned into *Sma*I-digested pBluescript SK+ (Stratagene). Site-directed mutagenesis was performed according to the method of Vandeyar et al. (*23*), employing the QuickChange site-directed mutagenesis kit (Stratagene). To produce the Y226L mutation, the *rbcL* gene sequence TAC (bases 676−678) was changed to TTA. This mutation introduced a *Dra*I restriction site that facilitated the screening of the transformants. Chloroplast transformation of the 18-7G strain with the resulting plasmid was performed via microprojectile bombardment. The transformation yielded photosynthesis-competent colonies. Successive rounds of single-colony isolation were performed to ensure homoplasmicity of the mutant genes. The *rbcL* mutant strain created by directed mutagenesis and transformation was named Y226L.

The small subunit mutations Y67A, Y68A, and Y72A were created by site-directed mutagenesis and transformation of a *C. reinhardtii* strain, which lacks the small subunit gene family (*20*), as described previously (*8*).

Rubisco Purification. Cells were collected by centrifugation at 2500*g* for 5 min. Pellets were weighed, frozen with liquid nitrogen, and stored at −80 °C.

Rubisco from different mutants was purified by previously reported procedures, including 35−60% ammonium sulfate fractionation, sucrose gradient centrifugation (*24*), and fast protein liquid chromatography (FPLC) with an anion exchanger column (*25*). The final protein preparation contained more than 95% rubisco, was essentially free of nucleic acids ($A_{280}/A_{260} > 1.7$), and did not undergo endogenous proteolysis under the conditions of the assays reported in this work. The amount of enzyme protein was determined from the optical density at 280 nm, assuming an average extinction coefficient ($\epsilon^{1\%}$) of 15.7 as reported for rubisco from several organisms (data reviewed in ref *10*).

Rubisco Carboxylase Activity Assay. The enzyme was transferred to activation buffer [100 mM Tris-HCl, 10 mM $MgCl_2$, and 10 mM $NaHCO_3$ (pH 8.2)] by gel filtration through a Sephadex G-25 column (Amersham Pharmacia Biotech PD-10). The rubisco carboxylase activity was determined by assessing the incorporation of acid stable ^{14}C from $NaH^{14}CO_3$ for 5 min (*24*).

Proteolytic Assay. Subtilisin digestion of rubisco was carried out according to a published procedure (*26*). Purified rubisco (0.2 mg/mL in activation buffer), from mutants and from wild-type transformants, was oxidized (treated with 20 mM disulfide cystamine) or reduced (treated with 40 mM free thiol cysteamine) for 2 h under a nitrogen atmosphere

before being incubated with subtilisin (0.5 μg/mL) at 30 °C for fixed amounts of time. The proteolytic reaction was stopped by adding phenylmethanesulfonyl fluoride (PMSF) at a final concentration of 22 mM and placing the samples on ice for 10 min. Afterward, the samples were boiled in a loading buffer and run on SDS−PAGE. The gels were stained with Coomassie Blue, and the bands were quantified by image analysis using Gel-Doc Quantity One from Bio-Rad.

Electrophoresis and Immunoblotting. Discontinuous SDS−PAGE (10% polyacrylamide in the resolving gel) and native polyacrylamide gradient gel electrophoresis (PAGGE) were carried out as previously detailed (*26*). The gels were either stained with 0.1% (w/v) Coomassie Blue R-250 in 20% methanol and 5% acetic acid or blotted onto polyvinyldifluoridene (PVDF) membranes and developed using a primary rabbit antibody raised against *Lemna* minor rubisco and a secondary goat anti-rabbit IgG antibody coupled to horseradish peroxidase (Bio-Rad).

In Vivo Stress Experiments. Liquid cultures growing at 25 °C on acetate medium under light were stressed at a cell density of $5-6 \times 10^6$ cells/mL by addition of H_2O_2 to a final concentration of 1.6 mM (weak stress) or 10 mM (strong stress) in the culture medium. The cells were incubated for a further 10 h under the same culture conditions, and cell samples were collected periodically throughout the stress process. The cells were sedimented by centrifugation (5000*g* for 2 min), resuspended in 80 mM Tris-HCl (pH 6.8), 0.1 M 2-mercaptoethanol, 2% (w/v) SDS, 15% (v/v) glycerol, and 0.006% (w/v) *m*-cresol purple, and boiled for 4 min. The samples were subjected to SDS−PAGE and immunoblotting and quantified by image analysis using Gel-Doc Quantity One from Bio-Rad.

RESULTS

Mutant Growth and Rubisco Level of Expression. The *RbcS*-T60-3 photosynthetic-deficient mutant of *C. reinhardtii* that lacks the two *RbcS* genes (*20*) was utilized for the transformation of the A−B loop small subunit mutants. The Y67A and Y68A mutants were obtained by transforming the host strain with the mutated *RbcS1* gene (*8*). The Y72A mutant was similarly recovered but using a mutated *RbcS2* copy (M. Anwaruzzaman and R. J. Spreitzer, personal communication). A parallel transformation of the same host strain with the wild-type *RbcS1* or *RbcS2* gene yielded transformants (named S1-Wt and S2-Wt, respectively) that were used as wild-type controls in both in vivo and in vitro experiments.

The Y226L large subunit mutant was obtained by transforming the nonautotrophic 18-7G *rbcL* mutant strain (*19*). A parallel transformation with wild-type *rbcL* was also carried out to obtain a wild-type control for Y226L (called L-Wt).

All transformant strains were selected as photosynthetically competent colonies growing on minimal medium, thereby demonstrating the capacity of all mutant rubiscos to assemble into functional holoenzymes. When growth rates were compared on solid minimal medium at 25 °C, only the Y72A mutant grew more slowly than the corresponding wild-type control (S2-Wt). However, on solid minimal medium at 35 °C, the growth of the Y67A, Y68A, and Y226L mutants was retarded, compared with their controls, and the Y72A strain seemed unable to grow.

Table 1: RuBP Carboxylase Activity of Rubisco Purified from the Mutant and Wild-Type Enzymes[a]

	RuBP carboxylase activity (μmol of CO_2 min^{-1} mg^{-1})	
strain	activity without CSH	activity with CSH
Y226L	0.724 ± 0.018	1.020 ± 0.016
L-Wt	2.276 ± 0.102	2.355 ± 0.068
Y72A	0.014 ± 0.001	0.008 ± 0.001
S2-Wt	1.619 ± 0.113	1.825 ± 0.039
Y68A	1.075 ± 0.051	1.160 ± 0.019
Y67A	0.008 ± 0.001	0.008 ± 0.001
S1-Wt	1.815 ± 0.093	1.979 ± 0.143

[a] Purified enzyme solutions (0.2 mg/mL in activation buffer) were incubated in the presence or absence of the free thiol cysteamine CSH (40 mM) at 30 °C for 2 h under a nitrogen atmosphere, before the RuBP carboxylase activity was measured at 30 °C. Values are the means of three replicates (±standard error).

Analyzed for rubisco content, the Y68A mutant had approximately the same amount of enzyme per cell than the S1-Wt control strain. In contrast, mutants Y67A and Y72A contained much less (~10%) rubisco than the wild-type strains, and the purification yields were particularly low. The Y226L mutant had a somewhat smaller amount of rubisco than the L-Wt control (~80% of the wild-type content).

Rubisco Activity and Thermal Sensitivity. To investigate the catalytic and structural effects of the tyrosine substitutions, rubisco was purified from all mutant and wild-type strains and assayed for RuBP carboxylase activity and thermal stability. Substantial differences in specific activity (determined at 30 °C) were found between several mutant enzymes and their wild-type controls (Table 1). Y68A exhibited ~60% of the specific activity of the wild-type enzyme; Y226L had ~30% of the control activity, and the Y67A and Y72A enzymes had a very low specific activity (less than 5% of that of the wild-type enzymes). To determine if the diminished specific activity of the mutant rubiscos could result from a special sensitivity to reversible oxidative inactivation, the purified enzymes were treated with 20 mM cysteamine (a reducing monothiol), but this led to an only partial recovery of activity (~30% increase) in the case of Y226L, without a significant effect on the other mutants (Table 1).

When the purified Y72A and Y226L rubiscos were incubated at elevated temperatures (50−61 °C), they inactivated at a lower temperature than the wild-type control enzymes (Figure 2). The midpoint of the transition to the inactive state was ~56 °C for the wild-type rubisco but ~54 °C (i.e., 2 °C lower) for the Y72A and Y226L enzymes (Figure 2). The thermal stability of the Y67A and Y68A rubiscos has been already investigated, and these mutant enzymes have been shown to be similarly sensitive to temperature (*8*).

Proteolytic Pattern and Kinetics. Degradation of native wild-type rubisco with a broad specificity protease, such as subtilisin, has been shown to produce a transient accumulation of fragments of 53 (band I) and 47 kDa (band II) derived from the large subunit (*26*). Band I is generated by a redox-independent removal of an N-terminal piece up to K18 (site I). Band II results from clipping at a loop between S61 and T68 (site II). Processing at this latter site is known to be

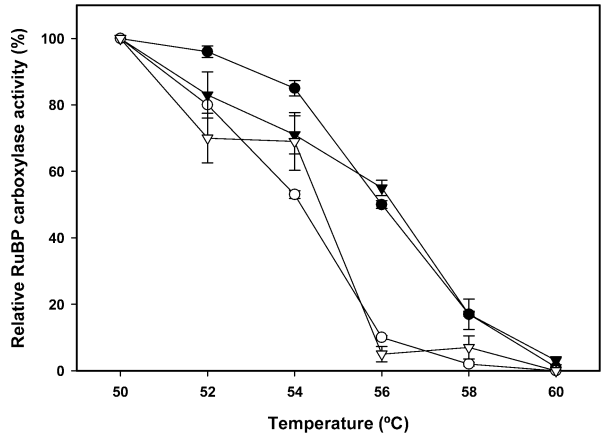

FIGURE 2: Thermal inactivation of rubisco purified from the wild-type (L-Wt and S2-Wt) and mutant (Y226L and Y72A) strains. Purified rubisco samples (0.2 mg/mL in activation buffer) were incubated at the indicated temperatures for 10 min. Afterward, the samples were placed on ice for 5 min and then incubated at 30 °C for the carboxylase activity assay. Activities are expressed as percentages of the activity measured for the enzyme incubated at 50 °C: wild-type L-Wt (▼), mutant Y226L (▽), wild type S2-Wt (●), and mutant Y72A (○). Values are the means of three replicates (±standard error).

greatly enhanced by oxidative modification of rubisco cysteines (*26*), producing a characteristic differential pattern of proteolysis between reduced and oxidized substrate (as seen in Figure 3 with the wild-type enzymes). Moreover, proteolytic cuts at site II in adjacent large subunits (i.e., those integrating the same dimer) have been suggested to trigger holoenzyme disassembly and, subsequently, unrestricted digestion of the released polypeptides (*26*).

A survey of the proteolytic patterns generated by subtilisin with the purified wild-type and mutant rubiscos is presented in Figure 3. All rubiscos were more sensitive to proteolysis under oxidizing than under reducing conditions. Also, all enzymes produced the characteristic bands I and II, except for the Y67A and Y72A mutant rubiscos, which were digested without accumulation of detectable fragments. Since band I and band II accumulate only while being integrated into the oligomeric holoenzyme (*26*), it appears that, in the case of Y67A and Y72A, subunit disassembly immediately followed the very first proteolytic cut, evidencing a certain weakness of the quaternary structure. On the other hand, even if the Y68A and Y226L rubiscos generated the expected fragments, some kinetic anomalies could be detected when compared with their wild-type counterparts. In the case of Y68A, the intact large subunit seemed to be more resistant to proteolysis. A careful inspection revealed that, in fact, only a certain percentage of the intact large subunits resisted digestion, while the rest was degraded at a faster pace. A plausible explanation for this behavior would be to have a certain fraction of the rubisco molecular population in an aggregated state, which would shield internal molecules from the action of the protease. Indeed, native electrophoresis of the Y68A rubisco revealed high-molecular mass noncovalent aggregates that disaggregated under SDS−PAGE conditions (Figure 4). As for the other mutant, the Y226L rubisco also exhibited an anomalous accumulation of band II (especially under reducing conditions) throughout proteolysis (Figure 3).

A mathematical model has been proposed to describe the amount of intact large subunit (z), and of band I (p_1) and

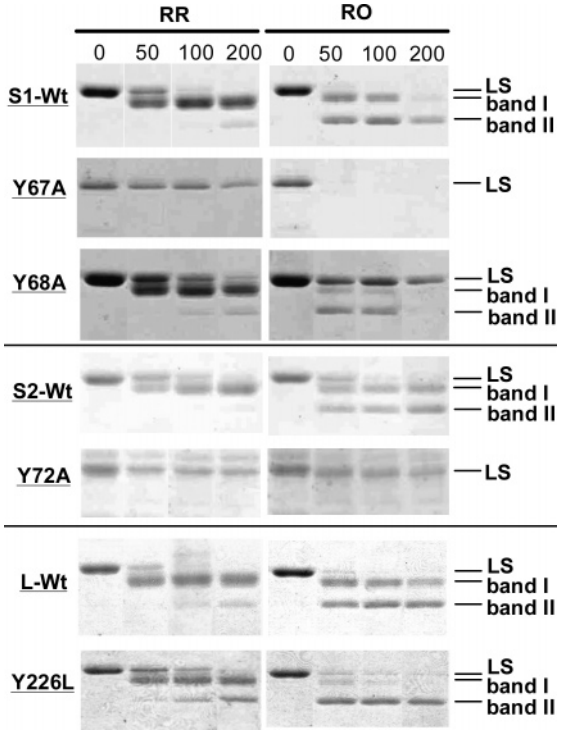

FIGURE 3: Subtilisin proteolysis of the rubisco large subunit from the wild-type (S1-Wt, S2-Wt, and L-Wt) and mutant (Y67A, Y68A, Y72A, and Y226L) strains under reducing (RR) or oxidizing (RO) conditions. Purified rubisco (0.2 mg/mL in activation buffer) was reduced or oxidized by a treatment with 40 mM cysteamine or 20 mM cystamine, respectively, for 2 h at 30 °C in a nitrogen atmosphere, before being incubated with subtilisin (0.5 μg/mL) at 30 °C for the indicated times (in minutes). The proteolytic products were run on SDS−PAGE gels and stained with Coomassie Blue. The positions of the intact large subunit (LS) and the proteolytic fragments of 53 (band I) and 47 kDa (band II) are indicated.

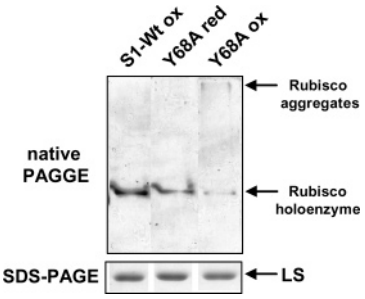

FIGURE 4: Aggregation of the Y68A mutant rubisco induced by oxidative treatment. Purified rubisco (0.2 mg/mL) from the S1-Wt or Y68A strain was reduced (Y68A red) or oxidized (S1-Wt ox and Y68A ox) as in Figure 3, and the samples were run on native PAGGE (top panel) and on SDS−PAGE (bottom panel). The positions of the Rubisco holoenzyme, Rubisco aggregates, and the large subunit (LS) are indicated.

band II (p_2) fragments, during proteolysis with subtilisin of the wild-type enzyme (*26*). The model uses four adjustable parameters in the form of the following kinetic constants: k_1 and k_2 for clipping of the intact large subunit at sites I and II, respectively; k_2' for the cut at site II of a large subunit that has been previously processed at site I; and k_3 for holoenzyme disassembly that leads to full proteolysis of the released subunits. We have adapted this model to fit the data of proteolysis of the mutant rubiscos to carry out a quantitative analysis of the observed anomalies.

In the cases of Y67A and Y72A, the intact large subunit (the one and only detectable large subunit band) decayed exponentially (Figure 5), as expected from the model. The corresponding first-order constant (named k_{tot}) might be compared to $8(k_1 + k_2)$, assuming that a single first cut (at site I or II) produces instantaneous disassembly of the native oligomer and full digestion of the eight large subunits integrating the holoenzyme. For Y67A in the reduced state, k_{tot} was even smaller than k_1 for the corresponding wild-type control (Table 2), indicating that the redox-independent processing at site I was hindered as a result of the mutation. In contrast, the value of k_{tot} for the oxidized Y67A was not significantly different from 8 times the sum of k_2 from the oxidized wild type and the diminished k_1 (i.e., $\sim^1/_8 k_{tot}$ from the reduced Y67A), suggesting that the mutation did not alter the redox-dependent processing at site II. On the other hand, k_{tot} for both the reduced and oxidized Y72A was definitely smaller than expected from the k_1 and k_2 values of the wild-type control (Table 2), implying that proteolysis at both sites was obstructed by the mutation.

The reduced Y68A exhibited a somewhat lower k_1 and a much higher k_3 compared to those of the wild type. Thus, like Y67A and Y72A, the mutation had the dual effect of impeding the processing at site I and facilitating holoenzyme disassembly. In the case of the oxidized Y68A, the presence of aggregated molecules that were resistant to proteolysis forced us to implement the model by introducing an undetermined percentage (q) of resistant molecules decaying at a slower rate, as simulated by a modulating factor (m) that acting on all proteolytic constants (k_1, k_2, and k_2') diminished their value ($m < 1$). With these two additional parameters (q and m), the fitting of the model to the experimental points was found to be satisfactory (Figure 5). The percentage of resistant (i.e., aggregated) molecules was determined to be 42%, and they were digested at ~2% of the overall rate of the free molecules (Table 2). Again, k_1 was lower and k_3 higher than in the corresponding oxidized wild-type enzyme, although the differences were not as marked as in the reduced state (Table 2).

The application of the same mathematical treatment to Y226L rubisco evidenced the presence of a minor fraction (between 20 and 30%) of proteolysis-resistant molecules in this mutant, too, in both the reduced and oxidized states (Table 2). However, these decayed at a rate faster than those of the oxidized Y68A, implying perhaps a smaller mean size of the aggregates. In addition, Y226L had increased values of k_2 and k_2', indicating an enhanced sensitivity of site II as a result of the mutation (Table 2). This, together with a slower disassembly (as shown by the lower k_3 values), promoted an exaggerated accumulation of band II as observed in either of the redox states (Figure 3).

Oxidative Stress Experiments in Vivo. Wild-type and mutant cultures were stressed with hydrogen peroxide, and the rubisco content of the cells throughout the stress process was analyzed by SDS−PAGE of whole cell extracts and immunoblotting with anti-rubisco antibodies. A weak oxidative stress (1.6 mM hydrogen peroxide) induced the breakdown of the wild-type rubisco into accumulating polypeptides with the following molecular masses: 44, 42, 37, and 28 kDa, the most abundant of them being the 37 kDa fragment (Figure 6A). Afterward, from 6−10 h of stress, the fragments declined, coinciding with the rise of rubisco aggregates on

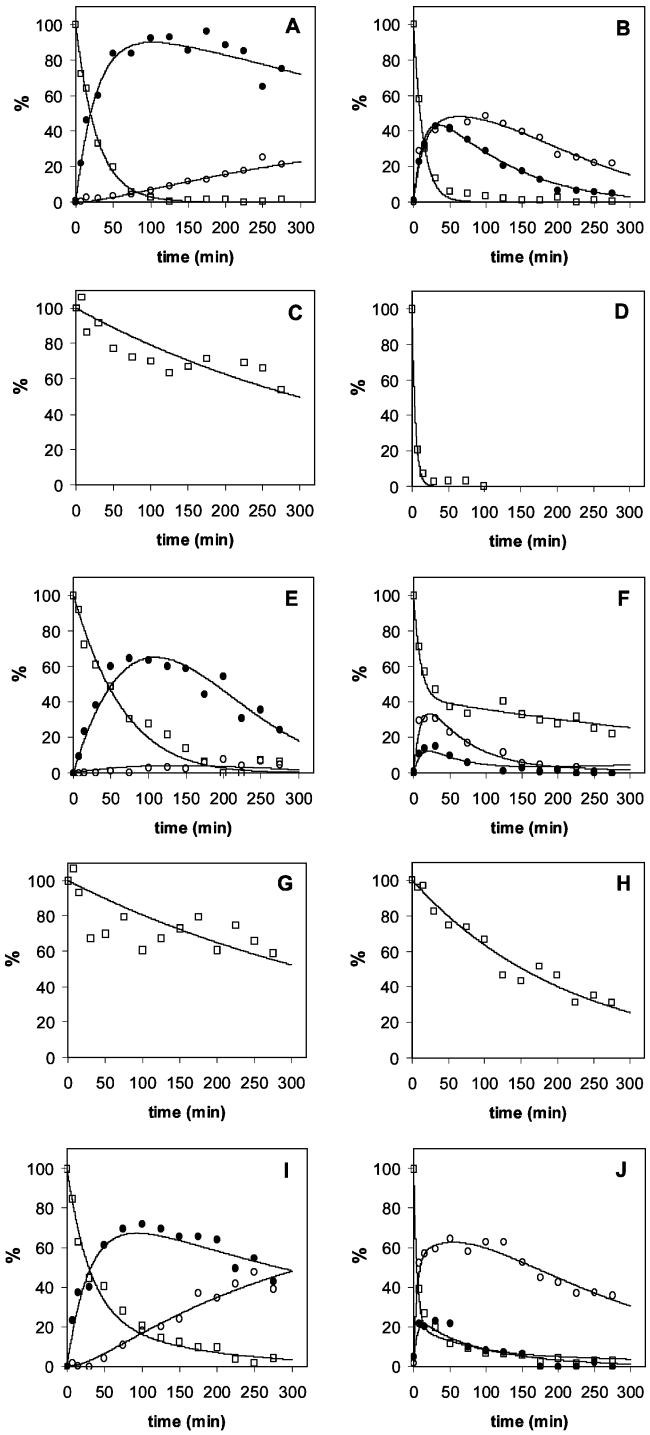

FIGURE 5: Time course of the amount of intact large subunit (□), band I (●), and band II (○) during in vitro proteolysis of the wild-type and mutant rubiscos. Purified rubisco (0.2 mg/mL) from S1-Wt (A and B), Y67A (C and D), Y68A (E and F), Y72A (G and H), and Y226L (I and J), previously reduced with 40 mM cysteamine (A, C, E, G, and I) or oxidized with 20 mM cystamine (B, D, F, H, and J) as in Figure 3, was incubated with subtilisin (0.5 μg/mL) at 30 °C for up to 275 min, and the proteolytic products were run on SDS−PAGE. The intact large subunit and its proteolytic fragments (band I and band II) were quantified from the gels stained with Coomassie Blue. The values obtained for band I and band II were normalized with respect to the intact large subunit by compensating for the loss of mass. Values are represented as percentages of the initial content of the intact large subunit. The curves fitting the experimental data were obtained by the model proposed by Marín-Navarro and Moreno (*26*) with auxiliary assumptions (see the text) and the kinetic constants given in Table 2.

Table 2: Estimated Values for the First-Order Rate Constants of the Proteolytic Kinetic Model for the Reduced (R) and Oxidized (O) Enzymes[a]

		S1-Wt	Y67A	Y68A	S2-Wt	Y72A	L-Wt	Y226L
R	k_1	0.036 ± 0.002	–	0.0143 ± 0.0014[b]	0.0114 ± 0.0009	–	0.0295 ± 0.0016	0.035 ± 0.014
	k_2	0	–	0.0007 ± 0.0002[b]	0	–	0	0
	k_2'	0.00101 ± 0.00012	–	0.0002 ± 0.0002[b]	0.00048 ± 0.00011	–	0.00106 ± 0.00013	0.0038 ± 0.0009[b]
	k_3	0.010 ± 0.016	–	1.6 ± 1.6	0	–	0.035 ± 0.012	0.001 ± 0.002[b]
	k_{tot}	–	0.0023 ± 0.0003	–	–	0.0022 ± 0.0003	–	–
	q	–	–	–	–	–	–	31 ± 24%
	m							(0.23 ± 0.06)
O	k_1	0.041 ± 0.003	–	0.028 ± 0.007[c]	0.011 ± 0.002	–	0.044 ± 0.005	0.07 ± 0.04
	k_2	0.034 ± 0.004	–	0.07 ± 0.02[c]	0.011 ± 0.003	–	0.032 ± 0.005	0.15 ± 0.09
	k_2'	0.0043 ± 0.0006	–	0.002 ± 0.002	0.0023 ± 0.0009	–	0.0025 ± 0.0005	0.012 ± 0.003[b]
	k_3	0.0125 ± 0.0007	–	0.032 ± 0.004[b]	0.0021 ± 0.0012	–	0.0088 ± 0.0010	0.0053 ± 0.0003[b]
	k_{tot}	–	0.21± 0.04	–	–	0.0046 ± 0.0003	–	
	q	–	–	42 ± 4%	–	–	–	20 ± 8%
	m			(0.016 ± 0.005)				(0.038 ± 0.016)

[a] Purified rubisco samples (0.2 mg/mL in activation buffer) were reduced or oxidized by incubation with 40 mM cysteamine or 20 mM cystamine, respectively, for 2 h at 30 °C under a nitrogen atmosphere, before being incubated with subtilisin (0.5 μg/mL). The kinetic constants (k_1, k_2, k_2', and k_3) were calculated by adjusting the mathematical model described by Marin-Navarro and Moreno (*26*) to the experimentally determined amounts of z (intact large subunit), p_1 (band I), and p_2 (band II) during subtilisin proteolysis, by minimizing the sum of square deviations. For the Y67A and Y72A strains, k_{tot} is the rate constant for the single-exponential decay of the intact large subunit. For Y226L and oxidized Y68A, the percentage of Rubisco resistant to proteolysis (q) is given, while the degree of resistance (m), evaluated as the ratio of the rate constants of the resistant fraction relative to the sensitive form, is also given. Each group of mutants with their wild-type counterpart is delimited by double lines to facilitate comparison. Since the values of the kinetic constants depend on the protease concentration, the experiments were performed with the same protease preparation for all the samples of the same group. Values of the first-order rate constants ± standard error are given in inverse minutes. [b] Statistically significant differences with the corresponding values of the wild-type enzymes are indicated (P > 99%). [c] Statistically significant differences with the corresponding values of the wild-type enzymes are indicated (P > 95%).

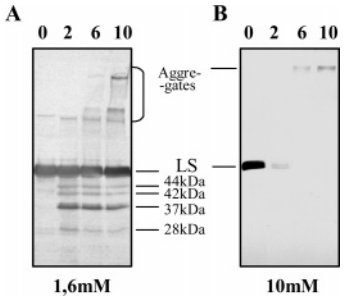

FIGURE 6: Evolution of large subunit aggregates and degradation fragments from rubisco in wild-type cells during weak (1.6 mM hydrogen peroxide) and strong (10 mM hydrogen peroxide) oxidative stress. Wild-type (S1-Wt) cells were stressed by addition of 1.6 (A) or 10 mM (B) hydrogen peroxide to the culture medium. At the indicated times, samples were taken and subjected to SDS−PAGE, transferred to a PVDF membrane, and probed with rubisco antibodies. The positions of the intact large subunit (LS), the high-molecular mass aggregates, and the molecular masses (in kilodaltons) of the degradation fragments are indicated.

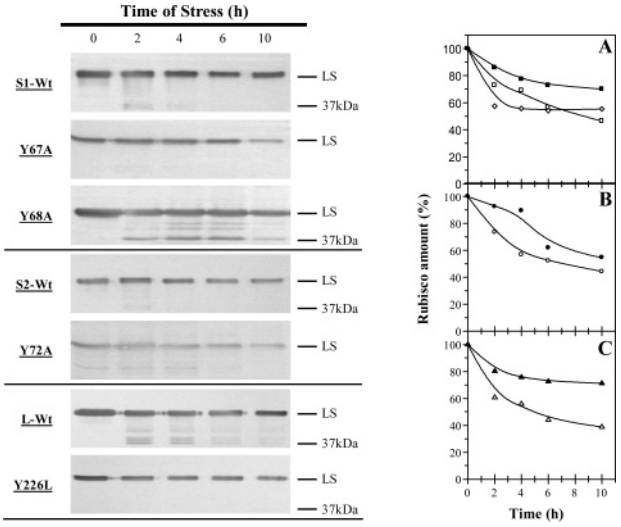

FIGURE 7: Degradation of rubisco in vivo under oxidative stress induced by 1.6 mM hydrogen peroxide. *C. reinhardtii* cells were stressed by addition of 1.6 mM hydrogen peroxide to the liquid culture medium. Cell samples were taken from the mutants (Y67A, Y68A, Y72A, and Y226L) and the respective wild-type controls (S1-Wt, S2-Wt, and L-Wt) at different times. Sample amounts corresponding to 1.3×10^5 (S2-Wt), 2.3×10^5 (S1-Wt), 7×10^5 (Y226L and L-Wt), 1.8×10^6 (Y68A), and 2.3×10^6 (Y67A and Y72A) cells were loaded for each strain. In the left panel, the samples were subjected to SDS−PAGE, transferred to a PVDF membrane, and probed with rubisco antibodies. The positions of the intact large subunit (LS) and the 37 kDa degradation fragment are indicated. In the right panel are the time courses of the rubisco content during in vivo degradation for the following strains: (A) Y67A (□), Y68A (◇), and S1-Wt (■), (B) Y72A (○) and S2-Wt (●), and (C) Y226L (△) and L-Wt (▲). The amount of intact large subunit remaining at each time (as determined by image analysis of the immunoblots) is represented as a percentage of the initial content.

the top portion of the immunoblot (Figure 6A). A higher concentration of hydrogen peroxide (10 mM) in the medium caused a fast disappearance of the large subunit without accumulation of detectable fragments, and the cross-linking of rubisco subunits into very high-molecular mass aggregates (Figure 6B). Because these aggregates did not penetrate the resolving gel or did not transfer efficiently, they were detected as a weak signal on top of the immunoblots (Figure 6B).

When subjected to oxidative stress (1.6 mM hydrogen peroxide), all tyrosine mutant strains were more sensitive than their wild-type counterparts, experiencing an enhanced degradation of rubisco, as witnessed by a faster decay of the large subunit signal in the immunoblots (Figure 7). Degradation was faster during the first 4 h of stress and progressed at a slower rate afterward. The decay of the Y68A rubisco gave rise to degradation fragments that were the same in size as those observed in the wild-type strains, whereas the rubisco from the other mutants (especially, Y67A and Y72A) was degraded without accumulation of detectable fragments (Figure 7).

DISCUSSION

As a general rule, the aromatic residues are buried in the interior of proteins, near other nonpolar side chains, and the resulting hydrophobic interactions contribute to the stabilization of the protein structure (*27*). The A−B loop of the small subunit of rubisco, located at the entrance of the central solvent channel, is rich in aromatic residues situated in the proximity of neighboring aromatic groups of the large subunit in the X-ray crystal structure of rubisco from *C. reinhardtii* (*6*, *7*). These aromatic interactions may presumably contribute to the overall structural stability of the oligomeric protein (e.g., by holding the large and small subunits together) and/or transmit concerted conformational changes between large and small subunits upon assembly into the native holoenzyme. We have selected for study four tyrosine residues located in the A−B loop (Y67, Y68, and Y72) or close to it, in the large subunit (Y226) (Figure 1). We have investigated their structural and functional relevance by replacing them with nonaromatic residues through site-directed mutagenesis and looking for phenotypic changes related to catalytic activity, thermal sensitivity, proteolytic susceptibility, and in vivo degradation of the enzyme under stress conditions.

Because the A−B loop domain has been originally related to holoenzyme assembly (*3*), it might have been expected that mutations in this region would hinder a proper incorporation of the small subunits into the large subunit core. However, the A−B loop mutants studied in this work did all assemble a functional holoenzyme, as observed in previous studies with similar substitutions in the A−B loop of the pea (*4*) and *C. reinhardtii* (*8*) rubiscos. In fact, only the replacement of Arg59 (Arg51 in land plants) with Glu has been shown to block holoenzyme assembly in the pea rubisco (*4*), while other substitutions within the A−B loop result in different degrees of thermal sensitivity and restricted growth at elevated temperatures (*8*). Among the mutants examined here, Y67A, Y68A, and Y226L grew with difficulty at 35 °C in minimal medium, while the Y72A mutant was unable to grow at 35 °C. In a previous work, the exchange of the amino acid residue preceding Y72, Arg 71, with alanine resulted also in a mutant strain (R71A) with restricted growth at 35 °C (*8*), evidencing that substitutions on the C-terminal part of the A−B loop can induce substantial structural changes in a way that decreases the thermal stability of the enzyme in vivo. Concurrently, all the mutant enzymes (Y67A, Y68A, Y72A, and Y226L) exhibited an associated thermal instability in vitro (ref *8* and Figure 2). The implication of tyrosines in thermal stabilization of proteins through aromatic−aromatic interactions has been described (*27*). As an example, a temperature-resistant lipase has recently been constructed with an asparagine to tyrosine substitution, thereby creating an additional aromatic−aromatic interaction with a neighboring tyrosine that produces a 10-fold increase in the half-life of the enzyme at 55 °C (*28*). Conversely, it is conceivable that the replacement of tyrosines with nonaromatic amino acids destabilizes rubisco structure by disrupting aromatic interactions in the vicinity of the mutated residue.

It seems, however, that the replacement of tyrosines in the rubisco mutants studied here not only eliminated stabilizing interactions but also promoted detectable conformational changes. This conclusion is supported by the alteration of both the specific carboxylase activity (Table 1) and the kinetics of proteolysis by subtilisin (Table 2). Furthermore, because both the catalytic center and the subtilisin-sensitive sites reside in the large subunit, these results demonstrate that the effects of substitutions at the A−B loop of the small subunit can spread to the large subunit as conformational alterations, as has been previously proposed (*8*) and recently proven (*29*). Indeed, the carboxylase activity was significantly reduced in all mutants (especially for Y67A and Y72A, falling below 5% of the wild-type activity), and it was not totally recovered by incubation with cysteamine, suggesting that the inactivation did not result from an increased level of exposure of critical cysteine residues to reversible oxidation (*24*). Thus, it appears that activity loss reflects rather a certain extent of conformational change that is propagated to the catalytic site.

On the other hand, the mutations also altered proteolytic kinetics in all cases. Because protease action can be used as a structural probe, we have adapted a previous mathematical model (*26*) to describe the proteolysis of mutant rubiscos to detect possible deviations due to structural constraints imposed by the site-directed mutations. The model gives an unbiased fit to the experimental points obtained by digestion of the mutant rubiscos with subtilisin (Figure 5) provided that a few auxiliary assumptions are introduced to take into account the absence of intermediary fragments (for Y67A and Y72A) or the aggregation propensity (for Y68A and Y226L). Detectable degradation products did not accumulate in rubisco mutants Y67A and Y72A, probably because of the immediate dismantling of the holoenzyme upon the first proteolytic cut. Mutants Y68A and Y226L also exhibited significant differences with the wild type in some of the kinetic constants (Table 2) and were especially prone to aggregation. While alterations in the proteolytic pattern or kinetics surely result from conformational changes, this work validates the quantitative analysis of the digestion of rubisco mutants with subtilisin using a published model (*26*) as a sensitive tool for detecting structural modifications induced by the mutations.

To investigate the stability of the mutant rubiscos in vivo, the mutant cells have been exposed to oxidative stress caused by hydrogen peroxide. In wild-type cells, this stress induced rubisco breakdown, with accumulation of degradation fragments of definite size, the most abundant being a 37 kDa piece (Figure 6). Polypeptides of a similar size, resulting from rubisco degradation, have been described in pea (*30*), barley (*12*), wheat (*31*, *32*), and grapevine in vitro and ex vitro (*33*). The high-molecular mass aggregates detected at a later phase of the oxidative stress (Figure 6) were also observed by Li et al. (*34*) when purified rubisco was treated with hydrogen peroxide for several hours. All tyrosine mutants exhibited enhanced rubisco degradation under stress conditions (Figure 7). Detectable breakdown products under stress did not accumulate in most of them, suggesting that the enzymes may suffer a direct conversion to small oligopeptides and amino acids, as observed in the subtilisin proteolysis of purified rubisco from the Y67A and Y72A mutants (Figure 3). This is likely to be the consequence of a structural weakness caused by the mutations and leading to facilitated subunit disassembly and enhanced turnover, in agreement with the low stationary level of rubisco kept by these mutants

under nonstress conditions. In this regard, the substitution of Y67 and Y72 seems to be the more destabilizing because these mutant rubiscos display the lowest thermal and proteolytic stability and are present at a very low stationary level in unstressed cells. On the other side, the mutation of Y68 appears to be the milder replacement since the Y68A enzyme experiences only a moderate decrease in stability and specific activity. These results are in good agreement with the natural variability of amino acid sequence observed in photosynthetic eukaryotes at these positions. A survey of the amino acid sequences of small subunit Rubiscos aligned according to structural criteria (*8*), and a similar alignment for large subunit sequences, indicated that tyrosine was present in a vast majority of cases. Remarkably, only conservative replacements of tyrosine with another aromatic residue (phenylalanine) were observed for Y67 (*Cucumis*), Y72 (*Porphyridium*), and Y226 (*Cucumis*, *Gossypium*, *Porphyridium*, and *Cylindrotheca*), whereas substitution with a nonaromatic residue (glutamine) was allowed for Y68 (*Acetabularia* and *Amaranthus*). This suggests that the involvement of Y68 in aromatic cluster interactions is less relevant to the functional features of Rubisco than the contribution of the other residues that we have studied.

We conclude that the tyrosines from the aromatic cluster around the A−B loop play an important structural role at the large subunit−small subunit hinge. Their replacement with nonaromatic amino acids results in conformational changes that influence rubisco structural stability, enzymatic activity, and in vivo degradation. This work demonstrates that the modification of rubisco catabolism in vivo may be achieved by exchanging residues other than cysteines. Furthermore, it shows that the rate of rubisco degradation under stress conditions can be altered by replacing residues from the small subunit. This confirms the physiological relevance of the structural role played by the small subunit and identifies a potential target for an eventual biotechnological manipulation of rubisco catabolism and level of expression.

ACKNOWLEDGMENT

We thank Dr. Robert J. Spreitzer (Department of Biochemistry, University of Nebraska, Lincoln, NE) for providing the site-directed mutants of tyrosines in the A−B loop of rubisco small subunit and their corresponding wild-type controls and for helpful discussions.

REFERENCES

1. Spreitzer, R. J., and Salvucci, M. E. (2002) Rubisco: Structure, regulatory interactions, and possibilities for a better enzyme, *Annu. Rev. Plant Biol. 53*, 449−475.
2. Knight, S., Andersson, I., and Brandén, C.-I. (1990) Crystallographic analysis of ribulose 1,5-bisphosphate carboxylase from spinach at 2.4 Å resolution, *J. Mol. Biol. 215*, 113−160.
3. Wasmann, C. C., Ramage, R. T., Bohnert, H. J., and Ostrem, J. A. (1989) Identification of an assembly domain in the small subunit of ribulose-1,5-bisphosphate carboxilase, *Proc. Natl. Acad. Sci. U.S.A. 86*, 1198−1202.
4. Flachmann, R., and Bohnert, H. J. (1992) Replacement of a conserved arginine in the assembly domain of ribulose-1,5-bisphosphate carboxylase/oxygenase small subunit interferes with holoenzyme formation, *J. Biol. Chem. 267*, 10576−10582.
5. Spreizer, R. J. (2003) Role of the small subunit in ribulose-1,5-bisphosphate carboxylase/oxygenase, *Arch. Biochem. Biophys. 414*, 141−149.
6. Taylor, T. C., Backlund, A., Bjorhall, K., Spreitzer, R. J., and Andersson, I. (2001) First crystal structure of Rubisco from a green alga, *Chlamydomonas reinhardtii*, *J. Biol. Chem. 276*, 48159−48164.
7. Mizohata, E., Matsumura, H., Okano, Y., Kumei, M., Takuma, H., Onodera, J., Kato, K., Shibata, N., Inoue, T., Yokota, A., and Kai, Y. (2002) Crystal structure of activated ribulose-1,5-bisphosphate carboxylase/oxygenase from green alga *Chlamydomonas reinhardtii* complexed with 2-carboxyarabinitol-1,5-bisphosphate, *J. Mol. Biol. 316*, 679−691.
8. Spreitzer, R. J., Esquivel, M. G., Du, Y. C., and McLaughlin, P. D. (2001) Alanine-scanning mutagenesis of the small-subunit βA-βB loop of chloroplast ribulose-1,5-bisphosphate carboxylase/oxygenase: Substitution at Arg-71 affects thermal stability and CO_2/O_2 specificity, *Biochemistry 40*, 5615−5621.
9. Evans, J. R., and Seeman, J. R. (1989) The allocation of protein nitrogen in the photosynthetic apparatus: Costs, consequences and control, in *Photosynthesis* (Briggs, W. R., Ed.) pp 183−205, Alan R. Liss Inc., New York.
10. Ferreira, R. B., Esquível, M. G., and Teixeira, A. R. (2000) Catabolism of ribulose bisphosphate carboxylase from higher plants, *Curr. Top. Phytochem. 3*, 129−165.
11. Garcia-Ferris, C., and Moreno, J. (1994) Oxidative modification and breakdown of ribulose-1,5-bishosphate carboxylase/oxygenase induced in *Euglena gracilis* by nitrogen starvation, *Planta 193*, 208−215.
12. Desimone, M., Henke, M., and Wagner, E. (1996) Oxidative stress induces partial degradation of the large subunit of ribulose-1,5-bisphosphate carboxylase/oxygenase in isolated chloroplasts of barley, *Plant Physiol. 111*, 789−796.
13. Desimone, M., Wagner, E., and Johanningmeier, U. (1998) Degradation of active-oxygen-modified ribulose-1,5-bisphosphate carboxylase/oxygenase by chloroplastic proteases requires ATP-hydrolysis, *Planta 205*, 459−466.
14. Albuquerque, J., Esquível, M. G., Teixeira, A. R., and Ferreira, R. B. (2001) The catabolism of ribulose bisphosphate carboxylase from higher plants. A hypothesis, *Plant Sci. 161*, 55−65.
15. Moreno, J., Penarrubia, L., and Garcia-Ferris, C. (1995) The mechanism of redox regulation of ribulose-1,5-bisphosphate carboxylase/oxygenase turnover. A hypothesis, *Plant Physiol. Biochem. 33*, 121−127.
16. Moreno, J., and Spreitzer, R. J. (1999) C172S substitution in the chloroplast-encoded large subunit affects stability and stress-induced turnover of ribulose-1,5-bisphosphate carboxylase/oxygenase, *J. Biol. Chem. 274*, 26789−26793.
17. Marcus, Y., Altman-Gueta, H., Finkler, A., and Gurevitz, M. (2003) Dual role of cysteine 172 in redox regulation of ribulose 1,5-bisphosphate carboxylase/oxygenase activity and degradation, *J. Bacteriol. 185*, 1509−1517.
18. Marin-Navarro, J., and Moreno, J. (2005) Cysteines 449 and 459 modulate the reduction−oxidation conformational changes of ribulose 1,5-bisphosphate carboxylase/oxygenase and the translocation of the enzyme to membranes during stress, *Plant, Cell Environ.* (in press).
19. Spreitzer, R. J., and Ogren, W. L. (1983) Rapid recovery of chloroplast mutations affecting ribulose bisphosphate carboxylase/oxygenase in *Chlamydomonas reinhardtii*, *Proc. Natl. Acad. Sci. U.S.A. 80*, 6293−6297.
20. Khrebtukova, I., and Spreitzer, R. J. (1996) Elimination of the *Chlamydomonas* gene family that encodes the small subunit of ribulose-1,5-bisphosphate carboxylase/oxygenase, *Proc. Natl. Acad. Sci. U.S.A. 93*, 13689−13693.
21. Spreitzer, R. J., and Mets, L. (1981) Photosynthesis-deficient mutants of *Chlamydomonas reinhardtii* with associated light-sensitive phenotypes, *Plant Physiol. 67*, 565−569.
22. Dron, M., Rahire, M., and Rochaix, J. D. (1982) Sequence of the chloroplast DNA region of *Chlamydomonas reinhardii* containing the gene of the large subunit of ribulose bisphosphate carboxylase and parts of its flanking genes, *J. Mol. Biol. 162*, 775−793.
23. Vandeyar, M. A., Weiner, M. P., Hutton, C. J., and Batt, C. A. (1988) A simple and rapid method for the selection of oligodeoxynucleotide-directed mutants, *Gene 65*, 129−133.
24. Garcia-Ferris, C., and Moreno, J. (1993) Redox regulation of enzymatic activity and proteolytic susceptibility of ribulose-1,5-bishosphate carboxylase/oxygenase from *Euglena gracilis*, *Photosynth. Res. 35*, 55−66.
25. Esquível, M. G., Ferreira, R. B., and Teixeira, A. R. (1998) Protein degradation in C3 and C4 plants with particular reference to

ribulose bisphosphate carboxylase and glycolate oxidase, *J. Exp. Bot. 49*, 807−816.
26. Marin-Navarro, J., and Moreno, J. (2003) Modification of the proteolytic fragmentation pattern upon oxidation of cysteines from ribulose 1,5-bisphosphate carboxylase/oxygenase, *Biochemistry 42*, 14930−14938.
27. Burley, S. K., and Petsko, G. A. (1985) Aromatic−aromatic interaction: A mechanism of protein structure stabilization, *Science 229*, 23−28.
28. Acharya, P., Rajakumara, E., Sankaranarayanan, R., and Rao, N. M. (2004) Structural basis of selection and thermostability of laboratory evolved *Bacillus subtilis* lipase, *J. Mol. Biol. 341*, 1271−1281.
29. Karkehabadi, S., Taylor, T. C., Spreitzer, R. J., and Andersson, I. (2005) Altered intersubunit interactions in crystal structures of catalytically compromised ribulose-1,5-bisphosphate carboxilase/oxygenase, *Biochemistry 44*, 113−120.
30. Bushnell, T., Bushnell, D., and Jagendorf, A. (1993) A purified zinc protease of pea chloroplasts, EP1, degrades the large subunit of ribulose-1,5-bisphosphate carboxylase/oxygenase, *Plant Physiol. 103*, 585−591.
31. Ishida, H., Nishimori, Y., Sugisawa, M., Makino, A., and Mae, T. (1997) The large subunit of ribulose-1,5-bisphosphate carboxylase/oxygenase is fragmented into 37-kDa and 16-kDa polypeptides by active oxygen in the lysates of chloroplasts from primary leaves of wheat, *Plant Cell Physiol. 38*, 471−479.
32. Luo, S., Ishida, H., Makino, A., and Mae, T. (2002) Fe^{2+}-catalyzed site-specific cleavage of the large subunit of rubisco 1,5-bisphosphate carboxylase close to the active site, *J. Biol. Chem. 277*, 12382−12387.
33. Carvalho, L. C., Esquível, M. G., Martins, I., Pinto Ricardo, C., and Amâncio, S. (2005) Monitoring the stability of rubisco in micropropagated grapevine (*Vitis vinifera* L.) by two-dimensional electrophoresis, *J. Plant Physiol. 162*, 365−374.
34. Li, S., Lu, W., Li, G.-F., Gong, Y.-D., Zhao, N.-M., Zhang, R.-X., and Zhou, H.-M. (2004) Interaction of hydrogen peroxide with ribulose-1,5-bisphosphate carboxylase/oxygenase from rice, *Biochemistry (Moscow) 69*, 1136−1142.

BI052588Y